Ab initio investigation of structural, elastic, dynamic, and electronic properties of YN binary rare earth nitride in ZB cubic phase

A. Kadri[a], H. Sediki[b,c], S. Hiadsi[a] and M. Elchikh[d]

[a]*Electron Microscope and Materials Science Laboratory, University of Science and Technology Mohamed Boudiaf, Physical Engineering Department, BP 1505 El Mnaouar, Oran, Algeria.*
[b]*LCPM, Chemistry Department, Faculty of Exact and Applied Sciences, University of Oran 1, Ahmed Ben Bella, Algeria.*
[c]*Department of Materials Technology, Faculty of Physics, University of Science and Technology Mohamed Boudiaf, Algeria.*
[d]*Materials and Fluids Physics Laboratory, Faculty of Physics, University of Science and Technology of Oran, USTO-MB, Oran, BP 1505 Oran El Mnaouar, Algeria.*

Received 12 February 2024; accepted 27 June 2024

This research employs ab initio calculations, utilizing the FP-LAPW method as implemented in WIEN2k and the PP-PW method in QUANTUM ESPRESSO, within the framework of the GGA-PBE approximation, to investigate the physical properties of the rare earth nitride binary YN. Structural parameters of YN are determined, yielding predictive results consistent with recent calculations. Furthermore, a comprehensive investigation into mechanical behavior and elastic properties confirms the mechanical stability of YN in its cubic ZB structure. An analysis of the anisotropy coefficient reveals its elastic anisotropy. The dynamic stability of YN is investigated through PW_{-scf} calculations using DFPT theory, enabling the calculation of phonon spectra, frequencies, and polarization vectors. These findings affirm the dynamic stability of A material in the B3 structure. Electronic properties are probed, showing semiconductor behavior, utilizing GGA mBJ, and YS PBE0 methods to ascertain band gap values in the B3 structure. This suggests its potential for adoption in optoelectronic and phononic devices.

Keywords: DFT; DFPT; FP-LAPW; PP-PW; phonons; GGA; YN.

DOI: https://doi.org/10.31349/RevMexFis.70.060502

1. Introduction

Researchers and scientists consistently strive to discover and synthesize novel materials whose properties align with technological advancements and cater to various applications, including electronic and optoelectronic devices, as well as medical and biophysical applications. Among materials of industrial and technological interest, rare earth nitrides have attracted considerable attention and are presently experiencing rapid growth due to their varied structural [1], electronic [2-4], magnetic [5,6], thermoelectric [7] and phononic [8-10] properties, particularly in the context of their applications within semiconductor [11], magnetic [12], spintronic [4,13,14], and optoelectronic devices [15,16]. Applications of these materials necessitate a profound understanding of their crucial properties. In most cases, extracting these materials from nature proves challenging, particularly for rare earths containing significant amounts of radioactive elements like uranium and thorium. These elements can lead to contamination of air, water, soil, and groundwater [17]. Moreover, experimental study of the properties of most rare earth nitrides is challenging due to their inherent instability under ambient conditions [18].

The rare earth nitrides are nitrogen-based compounds containing elements of rare earth. They can be classified into several groups based on the number of constituents. Rare earth nitrides are prepared through various methods, including the mixing of powders of rare earth oxide and carbon in a nitrogen flow at a high temperature of 1500°C. Subsequently, the rare earth nitride is obtained through the intermediate stage of rare earth carbide [19].

Recently, researchers have turned to theoretical studies and results to apply them in scientific and industrial domains, especially with the advancement of computing technology [20-22]. Theoretical studies rely on simulation programs and high-capacity devices to investigate the properties and diverse structures of materials. Furthermore, these approaches have significantly lowered the research expenses [23].

The aim of our work is to achieve a better understanding of the properties of Yttrium Nitride compound in the Zinc Blende (B3) phase and give more accurate predictive results related to structural properties (lattice parameter, structural stability…), elastic properties (elastic constants, Young's modulus…), vibrational properties (dynamic stabilities, vibration modes…) and electronic properties (band energy, DOS…). These investigations of YN properties open avenues for its use in a wide range of technologies, including semiconductors, electronic, optoelectronic, and acoustic devices.

This work is divided into three sections, the first section reviews the theoretical foundations that form the basis of the calculation methods used in this work. The second section

presents our results, their interpretation, and a comparison with relevant works. Finally, we conclude this work with a conclusion.

2. Computational methodology

The calculations in our study are conducted using first-principles methodologies. Structural, mechanical, and electronic properties of Yttrium Nitride are computed employing the linearized augmented plane wave (FP-LAPW) method [24] within the framework of density functional theory (DFT) implemented in the WIEN2k code [25]. Wave functions, electron densities, and potentials are expanded with a maximum angular momentum $l_{\max} = 10$ inside muffin-tin spheres (RMT) and in a Fourier series in the interstitial region with a cutoff radius $\mathrm{RMTK}_{\max} = 8.5$. Self-consistent calculations have converged with an energy convergence of 0.1 mRy. The choice of K-points for irreducible Brillouin zone integration was made using the Monkhorst-Pack technique [26]. For the cubic binary phase B3, a $10 \times 10 \times 10$ mesh with 1000 points was employed. However, for elastic and electronic property calculations of the studied compound, a 5000 K-point grid with a $(17\times17\times17)$ mesh was used. The pseudopotential plane-wave (PP-PW) method based on density functional perturbation theory (DFPT) [27] implemented in the Quantum-ESPRESSO (QE) [28,29] code was utilized for lattice dynamic properties calculations. A $4\times4\times4$ q-point grid was employed for phonon calculations. In this study, the generalized gradient approximation (GGA) [30] was applied for the exchange-correlation potential treatment.

3. Results and discussion

3.1. Structural properties and mechanical stability

The structure of ZnS (Zinc-Blende) is formed due to the expansion of the NaCl phase. In this structure, the Y atom creates a face-centered cubic (FCC) lattice, and the N atom occupies a tetrahedral site within this lattice, with a space group (216) F-43m. The atom positions are as follows [31]: Y (0 0 0), N (1/4,1/4,1/4). In this part, we aim to determine the structural properties of the Yttrium Nitride compound within the cubic B3 phase (Zinc Blende ZnS), specifically investigating the lattice parameter a, the bulk modulus B0 and its derivative B. The results for these properties, calculated for YN nitride in this phase, are detailed in Table I. The structural parameters were calculated by adjusting the total energy (E_{tot}) of the system based on different volume values, using the Murnaghan equation of state (EOS) [32].

TABLE I. Lattice parameter a, the bulk modulus B_0 and its derivative B' for the YN material in the cubic B_3 phase.

	A (Å)	$B0$ (GPa)	B' (GPa)
YN-B3	5.286	113.459	4.013
	5.28 [33]	110 [33]	4.39 [33]
	5.19669 [34]	121[34]	3.74965 [34]
	5.294 [34]	107.07 [34]	3.60269 [34]

In comparison, our results for the lattice parameter in the $B3$ phase align well with theoretical findings [33,34]. Additionally, the calculated bulk modulus value for the YN compound shows good agreement with other references, with an average difference of 3.14% compared to the values calculated by Mancera *et al*. [33] using the same method as in this study, 6.64% compared to Cherchab *et al*. [34] results calculated using the LDA method, and an average difference of 5.6% compared to those calculated using the GGA method for the B3 phase. Similarly, the derivative value B' is consistent with Mancera *et al*. [33] findings, differing by 8.59%, as well as with Cherchab *et al.* [34] findings, differing by 7.09% calculated using the LDA approximation and by 11.4% using the GGA approximation.

The examination of elastic properties is crucial for comprehending the physical characteristics of solids, offering insights into the hardness and mechanical stability of materials [9]. The elastic constants are based on estimates of the deformation of a material in response to a given stress within the elastic deformation region. When dealing with materials exhibiting cubic symmetry, there are only three independent elastic constants: C_{11}, C_{12}, and C_{44}. The mechanical stability condition for these cubic materials was defined by Born and Huang [35]:

$$C_{11} - C_{12} > 0, \qquad C_{11} > 0, C_{44} > 0,$$
$$(C_{11} + 2C_{12}) > 0.$$

The bulk modulus is expressed in terms of C_{11} and C_{12} by the equation:

$$B = \frac{1}{3}(C_{11} + 2C_{12}).$$

The elastic constants are related to important mechanical parameters such as the shear modulus G, the Young's modulus E, the Poisson's ratio ν, and the anisotropy coefficient A.

The formulas to calculate these parameters are as follows:

$$G = \frac{(C_{11} + C_{12} + 3C_{44})}{5},$$
$$E = \frac{9BG}{3B + G},$$
$$\nu = \frac{3B - E}{6B},$$
$$A = \frac{2C_{44}}{C_{11} - C_{12}}.$$

Our obtained results for the elastic constants C_{11}, C_{12}, C_{44}, the bulk modulus B, shear modulus G, Young's modulus E, Poisson's ratio ν, and the anisotropy factor A for the YN material in the cubic phase B3, along with other theoretical findings, are presented in the Table II. The calculation

TABLE II. Elastic constants C_{ij} (GPa), bulk modulus B (GPa), shear modulus G (GPa), Young's modulus E, Poisson's ratio ν, anisotropy factor A, and the B/G ratio for the YN material in the cubic $B3$ phase. Values followed by [37] are from a previous work (Ref. [37]).

	$B3$
C_{11}	136.2489
	180 [GGA] [37]
	145.77 [LDA] [37]
	136.74 [GGA-SOL] [37]
C_{12}	103.485
	108.94 [GGA] [37]
	115.98 [LDA] [37]
	106.4 [GGA-SOL] [37]
C_{44}	76.83
	48.61 [GGA] [37]
	54.21 [LDA] [37]
	56.32 [GGA-SOL] [37]
B	114.406
	119.56 [GGA] [37]
	125.91 [LDA] [37]
	56.32 [GGA-SOL] [37]
G	41.839
	31.12 [GGA] [37]
	38.48 [LDA] [37]
	33.43 [GGA-SOL] [37]
E	111.878
	85.92 [GGA] [37]
	89.59 [LDA] [37]
	91.55 [GGA-SOL] [37]
ν	0.337
	0.38 [GGA] [37]
	0.38 [LDA] [37]
	0.37 [GGA-SOL] [37]
A	4.69
	3.052 [GGA] [37]
	3.639 [LDA] [37]
	3.712 [GGA-SOL] [37]
B/G	2.734
	3.841 [GGA] [37]
	3.272 [LDA] [37]
	3.485 [GGA-SOL] [37]

of these parameters was performed utilizing the FP-LAPW method implemented in the WIEN2k code package. From the Table II, it can be observed that the values of the elastic constants C_{11}, C_{12}, and C_{44} for the YN compound are positive, meeting the mechanical stability criteria for cubic crystal YN [36]. Furthermore, the C_{ij} constants in the B3 phase are consistent with the values obtained by the three methods GGA, LDA, and GGA-PBESOL as reported by Ghebouli *et al*. [37]. The bulk modulus, calculated from the elastic constants using the GGA method, is consistent with the value obtained through total energy minimization (EOS) in the cubic Zinc Blende phase, as indicated in Table I. The Pugh's ductility index B/G [38] is used to determine the ductile or brittle nature of a material, allowing differentiation between ductile and brittle behavior through the following relationship:

$$\text{Fragile} < B/G = 1.75 < \text{Ductile}.$$

This indicates that the YN material is ductile in the B3 phase. These results are in good agreement with other theoretical findings. The obtained value for the anisotropy coefficient A is shown in the table. It can be observed that $A > 1$ in the $B3$ phase, indicating that the YN compound has strong anisotropy in the Zinc Blende phase. The result obtained in this phase is consistent with the findings of Ghebouli *et al*. [37].

4. Phonon properties

The phonon properties play a crucial role in analyzing the performance and reliability of composites for structural applications [39]. Our work aims to analyze the phonon dispersion curve of the rare-earth-based binary material YN to determine its dynamic stability. We will examine the presence or absence of imaginary frequencies (negative frequencies) to assess whether the material is dynamically stable or unstable. Additionally, we will investigate the phononic modes at the gamma point, which is the center of the Brillouin zone, to gain a better understanding of the atomic vibration modes and their contribution to the dynamic behavior of the studied material.

We calculated the vibration frequencies and plotted the phonon dispersion curve of YN in the Zinc Blende cubic phase using the linear response method within the framework of density functional perturbation theory (DFPT) [27] and the quantum ESPRESSO code [28,29]. Additionally, we employed the generalized gradient approximation for the exchange-correlation potential.

The phonon dispersion curve with the corresponding Density of States (DOS) for the YN material in the cubic B3 phase (ZnS) is displayed in Fig. 1.

From the figure, it is evident that no imaginary phonon mode has been observed in the Brillouin zone for the B3 structure. Consequently, we can conclude that the YN material in the $B3$ structure is dynamically stable.

To further investigate the vibrational properties of this material, it is crucial to perform calculations of dielectric properties. These properties are associated with the system's response to an external field and have a significant impact near the center of the Brillouin zone. This influence results in the splitting of the longitudinal (LO) and transverse (TO) optical modes at the (Γ) point on the dispersion curve. We calculated the Born effective charge (Z*) and the dielectric constant (ϵ^{∞}) for the YN nitride in the B3 phase. Table III summarizes all our results along with other available data.

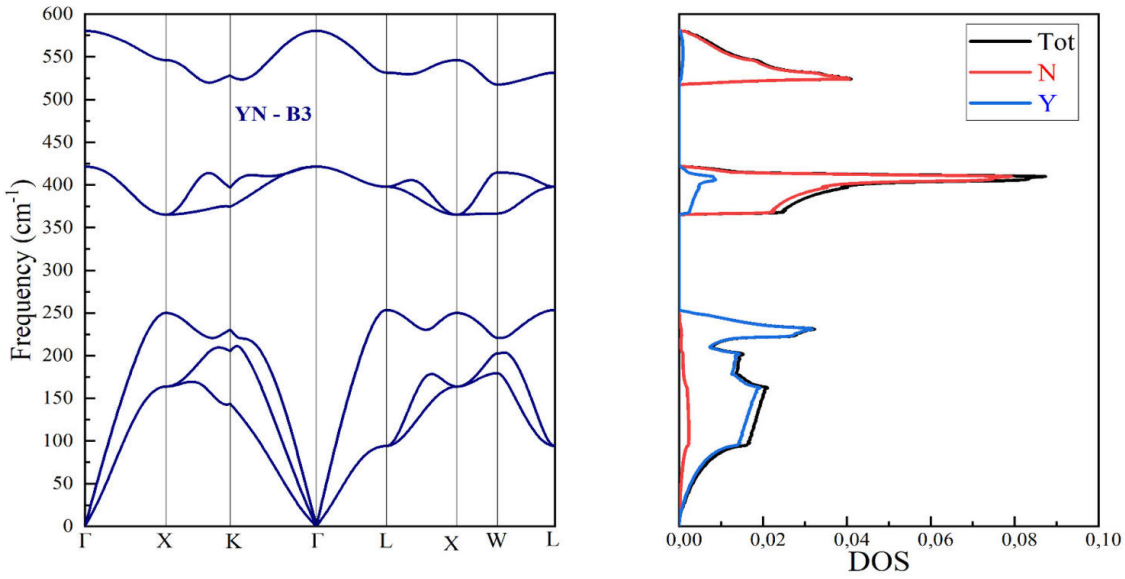

FIGURE 1. Phonon dispersion curve and total and partial density of states (DOS) curves of YN in the $B3$ phase.

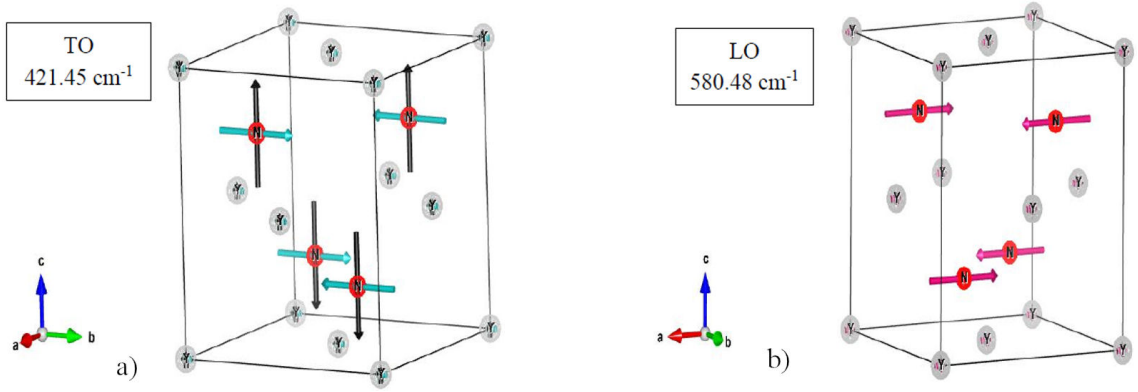

FIGURE 2. Polarization vectors of the optical phonon modes at the (Γ) point for the YN compound in the $B3$ phase.

TABLE III. Frequencies of longitudinal (LO) and transverse (TO) optical modes in (cm^{-1}) at the (Γ) point for YN in the B3 phase.

YN	B3
Γ_{TO}	421.45
	369 [37]
Γ_{LO}	850.48
	540 [37]

TABLE IV. Born effective charge Z^* (in Coulombs) and dielectric constant ϵ^{∞} for YN in the $B3$ phase.

YN	B3
Z^*	3.06
ϵ^{∞}	6.49

In evaluating the dynamic properties of YN in the $B3$ cubic phase, several key elements are considered for comparison with existing findings. Firstly, the acoustic branches are well separated from the optical branches, with gap of 111.84 cm^{-1}. This value is in good agreement with the calculated value of 127 cm^{-1} in reference [37]. Furthermore, there is a significant separation between longitudinal and transverse optical modes at the (Γ) point, with a frequency gap of 158.98 cm^{-1} for the B3 structure. The result from Ghebouli *et al.* [37] (66.2 cm^{-1}) is 58.35% lower than our obtained value. Analysis of the Phonon Density of States (PDOS) indicates that the N atom contributes to high-frequency phonon modes (optical modes) due to its low atomic mass, while the heavier Y atom dominates low-frequency phonon modes (acoustic modes). Additionally, the optical vibration modes at the (Γ) point for the $B3$ phase, as presented in Table IV, align with the results obtained in the other reference. The polarization vectors (Fig. 2) of the optical modes at the (Γ) point highlight the significant contribution of the N atom, with polarizations of $|P| = 0.98782$. It is worth noting that no other available results have been reported regarding the Born effective charge and the dielectric constant for the Zinc-Blende $B3$ phase of YN. After performing the phonon calculations for YN in the $B3$ phase, it is observed that the highest vi-

TABLE V. Direct and indirect energy gap values (in eV) of YN in the cubic $B3$ phase.

	$E^{W-\Gamma}$			E^{W-W}			$E^{\Gamma-\Gamma}$		
	GGA	mBJ	YSP-BE0	GGA	mBJ	YS-PBE0	GGA	mBJ	YS-PBE0
YN -B3-	2.05	3.9	3.135	2.244	3.734	3.34	3.508	5.328	4.841
				2.01[37]			3.35[37]		3.71[37]

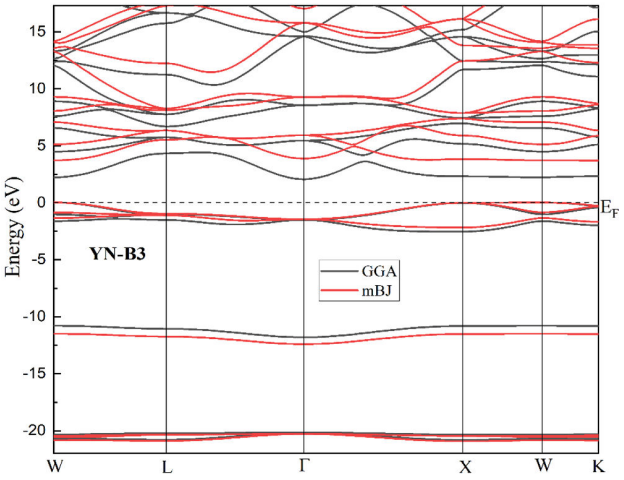

FIGURE 3. Band structure of YN in the B3 phase obtained by GGA and mBJ.

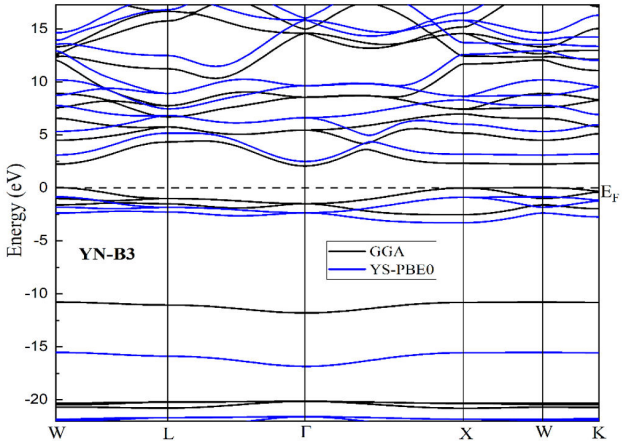

FIGURE 4. Band structure of YN in the $B3$ phase obtained by GGA and YS-PBE0.

bration corresponds to the optical mode at the Γ point with a frequency of 580.47 cm^{-1}.

5. Electronic properties

It is well-known that the GGA method underestimates band gaps in systems containing transition metal atoms with partially filled d and f orbitals [40]. To study the YN binary system, we employed two approximations: the modified Becke-Johnson (mBj) approximation [41] and the YS-PBEO hybrid exchange-correlation functional [42].

The calculations of electronic properties were conducted using the equilibrium lattice parameter obtained from the Murnaghan equation of state (EOS), and the energy band structure was plotted along the high-symmetry lines of the first Brillouin zone (BZ):

$$(w \rightarrow L \rightarrow \Gamma \rightarrow X \rightarrow W \rightarrow K).$$

The energy band structure of the YN compound in the $B3$ phase, obtained through three calculation methods, is illustrated in the Figs. 3 and 4.

In this phase, the Zinc Blende YN material is a semiconductor with a direct gap at the W point, as calculated by the mBJ method. However, with GGA and YS-PBE0, it exhibits an indirect semiconductor gap. This observation is consistent with the findings of Ghebouli *et al.* [37].

The results regarding the energy gaps obtained through the GGA, mBJ, and YS-PBE0 methods are compiled in Table V. To compare the results obtained by the three calculation methods, we plotted a zoom of the YN band structure from -3 to 5 eV (Fig. 5). From the figure, it can be observed that the mBJ approach provides a better energy gap compared to the other approximations.

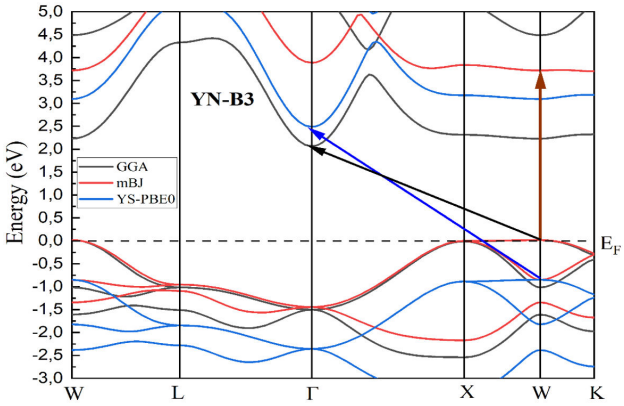

FIGURE 5. Zoom of the band structure of YN in the $B3$ phase obtained by GGA, mBJ, and YS-PBE0.

Furthermore, to comprehend and elucidate the contribution of states in the band structure and analyze the type of hybridization, we calculated the total and partial density of states (DOS) spectra for YN in the $B3$ structure using the GGA, mBJ, and YS-PBE0 approximations.

The results of the total (TDOS) and partial density of states (PDOS) for Yttrium Nitride compound in the $B3$ structure are illustrated in the Figs. 6-8.

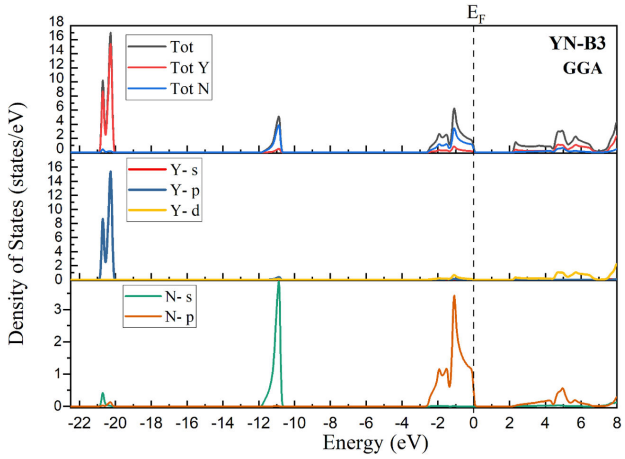

FIGURE 6. Total and partial density of states of YN in the $B3$ phase obtained using GGA.

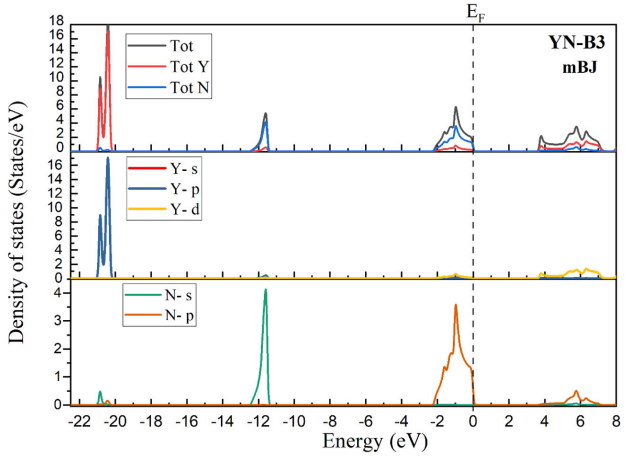

FIGURE 7. Total and partial density of states of YN in the $B3$ phase obtained using mBJ.

The density of states spectra for YN in the $B3$ phase is similar for all three calculation methods, as observed in the figures. We identified three significant valence regions. The first, deepest region is predominantly influenced by the p state of the Y atom, with a substantial contribution. The second region is dominated by the s state of the N atom (spanning approximately -13 eV to -11 eV). The third region corresponds to the maximum of the valence band, with a width of approximately 2.5 eV for all three methods. This region

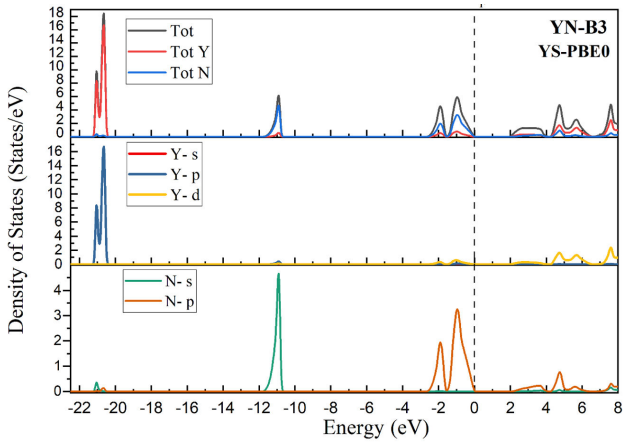

FIGURE 8. Total and partial density of states of YN in the $B3$ phase obtained using YS-PBE0.

is characterized by a strong presence of p states from the N atom, with a slight contribution from the d and p states of the Y atom. The lower conduction band region ranges from 2 to 8 eV for both GGA and YS-PBE0 methods, and from $\sim$3.7 eV to 8 eV for the mBJ method. It is mainly composed of the d state of the Y atom and the p state of the N atom, with a slight contribution from the s state of the N atom and the d state of the Y atom. Results of the density of states are consistent with those obtained by Ghebouli *et al.* [37] calculated using the GGA and HSE Hybrid methods.

6. Conclusion

In summary, our ab initio simulations, utilizing DFT and DFPT methods in WIEN2k and Quantum ESPRESSO, explore the physical properties of Yttrium nitride YN. The structural results closely align with existing data. Our study on elastic properties reveals that the obtained elastic constants meet all criteria for mechanical stability in the $B3$ cubic structure, indicating the mechanical stability of YN in these configurations. Electronic calculations categorize YN as a semiconductor, indicating a direct gap of 3.734 eV in the mBJ method and indirect gaps of 2.05 eV and 3.13 eV with GGA and YS-PBE0, respectively. The absence of imaginary phonon modes in the B3 structure emphasizes the dynamic stability of YN.

1. A. H. Baghdad *et al.*, Study of phase transitions and lattice dynamics, elastic and electronic properties, bonding and weak interactions analysis of YCuS2 in P212121, I4$^-$2d and P4$^-$21m space group structures. *Journal of Physics and Chemistry of Solids*, **167** (2022) 110756.
2. C. M. Aerts, P. Strange, M. Horne, W. M. Temmerman, Z. Szotek, and A. Svane, Half-metallic to insulating behavior of rare-earth nitrides. *Physical Review B*, **69** (2004) 045115.
3. L. Tie-Yu, and H. Mei-Chun, Electronic structure of ScN and YN: density-functional theory LDA and GW approximation calculations. *Chinese Physics*, **16** (2007) 62.
4. B. J. Ruck, Spintronics Potential Of Rare-Earth Nitrides. In Nanomagnetism And Spintronics: Fabrication, Materials, *Characterization and Applications* (2011) 193.
5. A. Murugan, G. S. Priyanga, R. Rajeswarapalanichamy, and K. Iyakutti, Structural, electronic, mechanical and magnetic properties of rare-earth nitrides REN (RE= Ce, Pr, Nd): A first prin-

ciples study. *Materials Science in Semiconductor Processing* **41** (2016) 17-25.

6. D. L. Cortie *et al*., Intrinsic reduction of the ordered 4 f magnetic moments in semiconducting rare-earth nitride thin films: DyN, ErN, and HoN. *Physical Review B*, **89** (2014) 064424.
7. A. Haoui, M. Elchikh, and S. Hiadsi, Mechanical, optoelectronic and thermoelectric properties of the transition metal oxide perovskites ysco3 and lasco3: first principle calculation. *Physica B: Condensed Matter*, **654** (2023) 414732.
8. V. Mankad, S. K. Gupta, and P. K. Jha, Ab initio investigation on structural, electronic and lattice dynamical properties of MgN and GdN crystals. *Results in Physics*, **2** (2012) 34.
9. A. Kadri, S. Hiadsi, M. Elchikh, and S. Bahlouli, Investigation of structural, mechanical, dynamic stability and electronic properties of anti-perovskite nitrides ANLa3 (A= Al, Ga): a DFT and DFPT studies. *Physica Scripta*, **98** (2023) 055931.
10. S. Granville *et al*., Vibrational properties of rare-earth nitrides: Raman spectra and theory. *Physical Review B*, **79** (2009) 054301.
11. F. Natali *et al.*, Rare-earth mononitrides. *Progress in Materials Science*, **58** (2013) 1316.
12. K. Upadhya *et al*., Electronic structure of rare-earth semiconducting ErN thin films determined with synchrotron radiation photoemission spectroscopy and first-principles analysis. *Physical Review B* **105** (2022) 075138.
13. C. M. Aerts, P. Strange, M. Horne, W. M. Temmerman, Z. Szotek, and A. Svane, The Spintronic Properties of Rare Earth Nitrides (2003). arXiv preprint cond-mat/0308354.
14. M. P. Ghimire, and R. K. Thapa, Magnetic and Electronic Structure Calculations of Rare-Earth Nitrides. *Journal of Materials Science and Engineering. A* **1(1A)** (2011) 53.
15. K. P. O'Donnell, and B. Hourahine, Rare earth doped III-nitrides for optoelectronics. *The European Physical Journal-Applied Physics*, **36** (2006) 91-103.
16. B. U. Haq, A. Afaq, G. Abdellatif, R. Ahmed, S. Naseem, and R. Khenata, First principles study of scandium nitride and yttrium nitride alloy system: prospective material for optoelectronics. *Superlattices and Microstructures*, **85** (2015) 24-33.
17. V. Balaram, Rare earth elements: A review of applications, occurrence, exploration, analysis, recycling, and environmental impact. *Geoscience Frontiers*, **10** (2019) 1285-1303.
18. J. Yang, F. Gao, H. Wang, H. Gou, X. Hao, and Z. Li, Elastic properties and hardness calculations of lanthanide nitrides in rocksalt structure. *Materials Chemistry and Physics*, **119** (2010) 499-504.
19. Y. Hirayama, K. Suzuki, A. Fujita, and K. Takagi, Experimental investigation of nitrogenation process for heavy rare earth nitrides from their hydrides. *AIP advances*, **9** (2019).
20. P. Makkar and N. N. Ghosh, A review on the use of DFT for the prediction of the properties of nanomaterials. *RSC advances*, **11** (2021) 27897.
21. D. Glossman-Mitnik, (Ed.) Density Functional Theory: Recent Advances, New Perspectives and Applications (2022).
22. B. Guan *et al*., Density functional theory researches for atomic structure, properties prediction, and rational design of selective catalytic reduction catalysts: Current progresses and future perspectives. *Molecular Catalysis*, **510** (2021) 111704.
23. A. Kadri, H. Bouafia, and S. Hiadsi, Energetic, mechanical and dynamical stability, electronic and bonding properties of new antiperovskite nitrides Y3AlN and Y3GaN: DFT and QTAIM investigation. *Physica B: Condensed Matter*, **667** (2023) 415212.
24. G. K. Madsen, P. Blaha, K. Schwarz, E. Sjöstedt, and L. Nordström, Efficient linearization of the augmented plane-wave method. *Physical Review B*, **64** (2001) 195134.
25. P. Blaha, K. Schwarz, G. K. Madsen, D. Kvasnicka, and J. Luitz, wien2k. An augmented plane wave+ local orbitals program for calculating crystal properties, **60** (2001).
26. H. J. Monkhorst and J. D. Pack, Special points for Brillouin-zone integrations. *Physical review B*, **13** (1976) 5188.
27. S. Baroni, P. Giannozzi, and A. Testa, Green's-function approach to linear response in solids. *Physical review letters*, **58** (1987) 1861.
28. S. Baroni, S. De Gironcoli, A. Dal Corso, and P. Giannozzi, Phonons and related crystal properties from density-functional perturbation theory. *Reviews of modern Physics*, **73** (2001) 515.
29. P. Giannozzi *et al.*, Quantum Espresso: a modular and open-source software project for quantum simulations of materials. *Journal of physics: Condensed matter*, **21** (2009) 395502.
30. J. P. Perdew, K. Burke, and M. Ernzerhof, Generalized gradient approximation made simple. *Physical review letters*, **77** (1996) 3865.
31. C. Kittel, and P. McEuen, Introduction to solid state physics. (John Wiley & Sons 2018).
32. F. D. Murnaghan, The compressibility of media under extreme pressures. *Proceedings of the National Academy of Sciences*, **30** (1944) 244.
33. L. Mancera, J. A. Rodriguez and N. Takeuchi, First principles calculations of the ground state properties and structural phase transformation in YN. *Journal of Physics: Condensed Matter*, **15** (2003) 2625.
34. A. J. E. Rowberg, S. Mu, M. W. Swift, and C. G. Van de Walle, Structural, electronic, and polarization properties of YN and LaN. *Physical Review Materials*, **5** (2021) 094602.
35. M. Born, On the stability of crystal lattices. I. In Mathematical Proceedings of the Cambridge Philosophical Society **36** (1940) 160.
36. M. Born, and R. D. Misra, Mathematical proceedings of the cambridge philosophical society (1940).
37. M. A. Ghebouli *et al*., First-principles calculations to investigate structural, elastic, electronic, lattice dynamic and optical properties for scandium and yttrium nitrides in zinc blend structure. *journal of materials research and technology*, **14** (2021) 1958.
38. S. F. Pugh, XCII, Relations between the elastic moduli and the plastic properties of polycrystalline pure metals. *The London, Edinburgh, and Dublin Philosophical Magazine and Journal of Science*, **45** (1954) 823.
39. V. Panwar, and K. Pal, Dynamic mechanical analysis of clay-polymer nanocomposites. In Clay-polymer nanocomposites (Elsevier 2017) pp. 413-441.

40. P. Khatri, and M. N. Huda, Application of attractive potential by DFT+ U to predict the electronic properties of materials without highly localized bands. *Computational materials science*, **81** (2014) 290.

41. A. D. Becke, and E. R. Johnson, A simple effective potential for exchange. *The Journal of chemical physics*, **124** (2006).

42. J. Heyd, G. E. Scuseria, and M. Ernzerhof, Hybrid functionals based on a screened Coulomb potential. *The Journal of chemical physics* **118** (2003) 8207.